Moisture sources and transport pathways for spring and summer EF1+ tornadic thunderstorms in central and eastern China

Ruqian Zhang[1] and Ming Xue[2]

[1] Key Laboratory of Mesoscale Severe Weather/Ministry of Education, School of Atmospheric Sciences, Nanjing University, Nanjing, Jiangsu 210023, China

[2] Center for Analysis and Prediction of Storms and School of Meteorology, University of Oklahoma, Norman, OK 73072, USA

Corresponding author: Ming Xue (mxue@ou.edu)

Submitted to Quarterly J. Royal Meteorological Society

7 May 2025

Revised October 2, 2025, December 1, 2025.

Abstract

Low-level moisture is a crucial factor in tornadogenesis, yet the sources of moisture for tornadoes in China remain largely unexplored. This study investigates the moisture sources and transport pathways for spring and summer EF1+ tornadoes in northern (CNN), central (CNC), and southern China (CNS) from 1980 to 2021. Using the Hybrid Single-Particle Lagrangian Integrated Trajectory (HYSPLIT) model and a Lagrangian-based moisture uptake algorithm, we find that tornadoes in CNN and CNC are characterized by significant moisture recycling (~27.2% from CNN and ~51.0% from CNC), whereas tornadoes in CNS predominantly draw moisture from the South China Sea (~71.3%). Ten tornado moisture transport channels from different regions are identified using *k*-means clustering (3 for CNN tornadoes, 3 for CNC tornadoes and 4 for CNS tornadoes). Proportions of moisture uptake for each moisture channel are also quantified. Synoptic-scale patterns associated with moisture channels reveal that moisture transport pathways are significantly influenced by the activity of the western North Pacific subtropical high (WNPSH). When the WNPSH is anomalously strong, moisture is usually transported through pathways originating from the East China Sea, the southern part (south of 25°N) of the western North Pacific, and the South China Sea. Conversely, under the influence of monsoon flows and low-pressure systems over China, moisture channels predominantly originate from land and the Bay of Bengal.

KEYWORDS

Tornadoes, moisture sources, synoptic-scale circulations, HYSPLIT

1. Introduction

Tornadoes are violently rotating columns of air typically associated with a funnel-shaped cloud extending downward from the base of a parent cumulonimbus updraft (Markowski & Richardson 2010). They are among the most destructive severe weather phenomena associated with localized convective storms (Bluestein 2013), capable of causing extensive damage to human life and property. Tornadoes generally form in environments characterized by high vertical wind

shear, large convective instability, and abundant low-level moisture (Brooks et al. 1994; Markowski et al., 2002; Thompson et al., 2003; Coffer & Parker 2015; Zhang et al., 2023). Analysis of tornadic storm soundings by Fawbush and Miller (1952) revealed a moist layer at low levels with an average relative humidity as high as 85%. Abundant low-level moisture contributes to storm precipitation, which in turn increases the potential for evaporation and baroclinic generation of vorticity, thereby enhancing the likelihood of tornadogenesis (Brooks et al. 1994). The low-level moisture also ensures sufficient convective available potential energy (CAPE) for the storm updrafts that are important for supporting low-level flow convergence and vortex intensification. It also affects the lifting condensation level (LCL) of low-level air parcels and both CAPE and LCL are important parameters within the composite significant tornado parameter (STP) that has predictive skill for significant tornadoes (Thompson et al., 2003; Zhang et al., 2025). Advancing the skillful forecasting of tornadoes necessitates understanding the sources and transport mechanisms of boundary-layer moisture to regions of tornadic storms.

Two primary methods for identifying water vapor origins are Eulerian moisture budget analysis and the Lagrangian approach. From the Eulerian perspective, precipitation is determined by variations in precipitable water, local evaporation, and moisture convergence/divergence by large-scale circulation (Trenberth & Guillemot 1995). However, a limitation of Eulerian analysis is that moisture in the target region cannot be easily traced back to its source (Nie & Sun 2022). Lagrangian trajectory models, such as the Hybrid Single-Particle Lagrangian Integrated Trajectory (HYSPLIT) model (Stein et al. 2015), the Lagrangian particle dispersion (FLEXPART) model (Stohl et al. 2005), and the Lagrangian Analysis Tool (Sprenger & Wernli 2015), can be used to address this limitation. Using the HYSPLIT model, Molina and Allen (2019) revealed a seasonal cycle in the origins and advection patterns of moisture contributing to winter and spring tornadoes in the United States. They found that the Gulf of Mexico was the predominant moisture source, accounting for more than 50% of the total contribution. The western Caribbean Sea and North Atlantic Ocean also contribute to winter tornadoes, while land areas of the contiguous United States play a more influential role during late spring.

In China, tornadoes have also caused significant damage and fatalities. They typically occur in late spring and summer (Fan & Yu 2015), and their environments exhibit moderate to high low-level humidity (Zhang et al. 2023). While moisture sources for precipitation in China have been studied (Hua et al. 2017; Huang et al. 2018; Jiang et al. 2017; Nie and Sun 2022; Wang et al. 2023; Yao & Jiang 2023), the origins of boundary-layer moisture fueling tornadoes remain unexplored.

When studying the environments of significant tornadoes [those rated (E)F2 or greater] in China, Zhang et al. (2023) divided the country into northern (CNN), central (CNC), and southern China (CNS). They found that tornado environments in CNN are characterized by higher shear and lower humidity, those in CNC by moderate shear, CAPE, and humidity, and those in CNS by the most conducive humidity conditions, lower CAPE, and weak shear. The main synoptic backgrounds for tornadoes in the three subregions are the North China cold vortex (midlevel), the Meiyu frontal system, and tropical cyclones (Zheng 2020). Therefore, investigating and comparing moisture sources for tornado cases in CNN, CNC, and CNS are important. Such regional analysis provides a better understanding of the characteristics of moisture sources for tornadoes over China and the understanding can help predict/project tornado occurrences in these regions at time scales ranging from short-range, sub-seasonal, and seasonal to the climate time scales.

In this paper, a climatological dataset of 179 tornado cases from the spring and summer seasons between 1980 and 2021 is used to identify the moisture sources and transport pathways for tornadoes over China. The study aims to address the following questions: 1) What are the

distributions of moisture sources for tornadoes in CNN, CNC, and CNS? 2) What are the common moisture transport pathways for tornadoes in China? 3) What are the characteristics of moisture sources and the synoptic-scale patterns for each moisture transport pathway?

The rest of this paper is organized as follows. The data, Lagrangian model, and analysis methods employed in this paper are presented in Section 2. Section 3 shows the distributions for backward trajectories of tornado moisture and Section 4 presents the results of trajectory clustering. Characteristics of moisture sources along backward trajectories are detailed in Section 5. Anomalous synoptic-scale circulations associated with the moisture channels are discussed in Section 6. A summary and conclusions are provided in Section 7.

2. Data and methods

2.1 Data

Tornado records of China are not as comprehensive or reliable as those of the United States (Zhang et al., 2023). In this study, 179 tornado cases that are recorded in the spring and summer seasons are included. Information on earlier tornadoes is obtained from "The Collection of Meteorological Disasters Records in China" (Ding 2008), the "Yearbook of Meteorological Disasters in China" (China Meteorological Administration, 2005–2022) and some are from reports on the Internet, but the EF scales are not given in these sources. Yu et al. (2021) assessed tornado intensities using the EF scale based on damage indicators from the U.S. National Weather Service survey standard. In China, standardized tornado damage surveys were not implemented until 2012 (Zheng et al., 2016; Bai et al., 2017; Meng et al., 2018; Cai et al., 2021), and even then, these surveys have not always been comprehensive. Some later tornadoes are more carefully documented by the Foshan Tornado Research Center (Huang et al., 2019; Li et al., 2020; Cai et al., 2021; Zhi et al., 2022). Because weak tornadoes are more difficult to record completely, this paper only considers relatively strong tornadoes rated EF2+ from 1980 to 2001 and those rated EF1+ from 2002 to 2021, while no EF5 tornado has been recorded in China. Due to the limited number of operational weather radars, EF1 tornadoes were not reliably recorded before 2002. The reliability of weak tornado reporting was also relatively low. Therefore, only EF2+ tornadoes are considered from 1980 to 2001, while EF1 tornado cases are also included between 2002 and 2021. To assess the possible impact of not including EF1 tornado cases in the earlier period, we performed moisture analyses on the cases from the two periods separately and found no substantial differences between the two periods. Moisture sources are found to vary more substantially across tornadoes in different regions than across tornado intensities. The results for the separate periods are not shown. As the environments of typhoon tornadoes are often characterized by very different circulation patterns and environments (Edwards et al., 2012), typhoon tornadoes are removed from the dataset in this paper.

The fifth-generation European Centre for Medium Range Weather Forecasting (ECMWF) reanalysis data (ERA5; Hersbach et al. 2020) are used to drive the HYSPLIT model. The hourly ERA5 dataset has a horizontal resolution of 0.25°. The relatively high hourly resolution is very beneficial to the accuracy of the time integrated trajectories. Additionally, daily ERA5 dataset is used for composite circulation analyses of tornado moisture channels.

2.2 Backward trajectory calculations

Backward trajectories are generated using the HYSPLIT model. PySPLIT (Warner 2018), a Python-based package for generating HYSPLIT air parcel trajectories and along-trajectory meteorological data, is used to run the HYSPLIT model. Trajectory information is provided hourly by the HYSPLIT model.

Small spatial adjustments at the starting point can impact trajectory modeling, resulting in discernibly different paths, even if starting points begin within the same meteorological model grid cell (Stohl 1998). To reduce the sensitivity of trajectory modeling, a three-dimensional matrix is employed for each tornado event, similar to the approach of Molina and Allen (2019) and Molina et al. (2020). Each matrix contains 5 × 5 × 6 (150) points with a horizontal grid spacing of 0.1° centered on the tornado location and a vertical spacing of one-tenth of the height of the planetary boundary layer (HPBL) from the mid-HPBL level to the full HPBL level. HPBL is an output variable in ERA5, calculated based on the bulk Richardson number (Seidel et al., 2012), and has been shown to perform better than in other reanalyses (Guo et al., 2024). The Lagrangian residence time of moisture between evaporation from the lower surface and precipitation to the ground is 4–5 days (Läderach & Sodemann 2016). During this residence time, moisture undergoes various physical and dynamic meteorological processes in the atmosphere. The integration time length of the Lagrangian model is 120 hours in this study.

Tornadoes in CNN are often triggered by dry lines (dry fronts) and the associated strong boundary layer convergence (Yuan et al., 2023). Due to integration errors in the trajectory model, especially given the limited spatial and temporal resolutions of the data, some backward trajectories that originate near the front may be traced back into the cold and dry air behind the front, even though their starting points are on the warm and moist side. Such trajectories are not representative of the moist inflow air feeding the tornadic storms. In such cases, shifting the center of the starting point matrix eastward or southward toward the inflow direction, the backward trajectories can better reflect the tornado moisture source. Although a small number of cold dry trajectories are still present after such adjustments, they constitute only a minor portion of the total trajectories in the same tornado cases and cannot affect the primary conclusions of the analysis. Backward trajectories for tornadoes in CNN are generated with the above adjustments, when necessary, while those for tornadoes in CNC and CNS remain unchanged.

2.3 Moisture source attribution

The moisture uptake (MU) diagnostic, proposed by Sodemann et al. (2008), identifies sources of moisture along calculated trajectories. This diagnostic is based on the changes in specific humidity along trajectories. Many studies employ this diagnostic method to identify moisture sources for various meteorological events, such as snowfall or rainfall over China (Cheng et al., 2021; Huang et al., 2018; Yang et al., 2019). The specific humidity of an air parcel, measured every 6 hours along its trajectory, generally represents the net effect of evaporation (E) into and precipitation (P) forming within the air parcel (James et al., 2004; Stohl & James, 2004):

$$\frac{Dq}{Dt} \approx \frac{\Delta q}{\Delta t} = E - P \quad (g\ kg^{-1}\ (6\ h)^{-1}). \quad (1)$$

where $\Delta q > 0$ denotes a moisture increase and $\Delta q < 0$ represents a moisture decrease over a 6 h period:

$$\Delta q(t) = q\big(\vec{x}(t)\big) - q\big(\vec{x}(t-6\,h)\big). \quad (2)$$

Here, $\vec{x}(t)$ is the parcel position at time *t*. The assumption is that turbulent fluxes enable moisture exchange between an air parcel and the surrounding boundary layer air when the parcel enters the boundary layer. To ensure thermodynamic significance in the MU calculation, an evaporative threshold of $\Delta q \geq 0.2g\ kg^{-1}$ is set, as values of $\Delta q < 0.2g\ kg^{-1}$ are considered negligible (Sodemann et al., 2008; Molina & Allen, 2019). An MU location is identified along a trajectory if a moisture increase occurs ($\Delta q \geq 0.2g\ kg^{-1}$) and the altitude of the air parcel is below HPBL. A moisture increase above HPBL is assumed to be caused by other physical or numerical processes, such as convection, evaporation of precipitating hydrometeors, and subgrid-scale turbulent fluxes, rather than an evaporation source at the surface (Sodemann et al., 2008).

An air parcel can experience repeated evaporation and precipitation cycles during its multi-day journey. Due to precipitation occurring along the way, the moisture from earlier evaporative sources gradually has a diminishing impact on the precipitation at the destination. Hence, the meteorological event is a weighted sum of the previous MU. The fractional MU is the ratio of the uptake amount to the moisture in the air parcel. Moving forward in time, starting from the end point and progressing to the start point of the backward trajectory: At an uptake location *n* below HPBL, calculate the fractional contribution f_n of the uptake amount Δq_n to the moisture in the air parcel q_n as

$$f_n = \frac{\Delta q_n}{q_n}. \quad (3)$$

A new MU event reduces the importance of previous MU events and the fractional contributions of all moisture uptakes at previous times *m* are recalculated with respect to the new moisture uptake at time *n*:

$$f_m = \frac{\Delta q_m}{q_n}, \qquad m > n. \quad (4)$$

At the point of precipitation, the previous fractional MU in the air parcel is discounted due to the precipitation amount ($\Delta q \leq -0.2g\ kg^{-1}$):

$$\Delta q'_m = \Delta q_m + \Delta q_n \cdot f_m \quad \text{for all} \quad m > n. \quad (5)$$

The MU diagnostic is employed to identify moisture sources, and therefore, only the starting points of backward trajectories with relative humidity values of 65% or higher are considered in this study.

2.4 Trajectory clustering

To identify the main moisture transport pathways of tornadoes in China, *k*-means clustering (Wilks 2011) is employed to cluster mean trajectories of every matrix for the CNN, CNC, and CNS regions separately. Firstly, the two-dimensional trajectory data (latitude and longitude coordinates) are converted into one-dimensional Hausdorff distance data (Rote 1991). The Hausdorff distance between each pair of trajectories is calculated, resulting in a symmetric distance matrix. This matrix measures the similarity between trajectories. Then, this distance matrix is input into the *k*-means algorithm for clustering the trajectories.

3. Distributions of moisture transport trajectories and moisture origins for tornadoes

A total of 27450 parcels (8250/12000/7200 parcels from CNN/CNC/CNS regions) are released to track the tornado moisture sources. After applying the filtering criteria described in section 2.3, 25429 parcels (6810/11612/7007 parcels from CNN/CNC/CNS regions) remain. There is a high density of parcel trajectories both over land and sea for tornadoes in the CNN region (Figure 1a). On land, most trajectories are in eastern China, following a southwest-northeast orientation. This orientation may show that the atmospheric circulations affected by the distribution of plains in China influence the tornado moisture pathway, for it exhibits a similar southwest-northeast pattern. In maritime areas, air parcels are primarily distributed over the sea near the east coast of China. Most of the air parcels that reach tornadoes in CNC are primarily distributed over central and southern China, as well as the regions from the Bay of Bengal to the Indochina subcontinent, the South China Sea and the western North Pacific (Figure 1b). For tornadoes in CNS, trajectories are mostly concentrated over the South China Sea and thinly distributed over land (Figure 1c). Different trajectory distributions for tornadoes in CNN, CNC, and CNS are clearly influenced by geographic locations of the tornadoes and the atmospheric circulations that transport the moisture, resulting in quite distinct routes over land and sea. The concentration of trajectories in these areas highlights the key transport channels for tornado moisture, which will be discussed in more detail next.

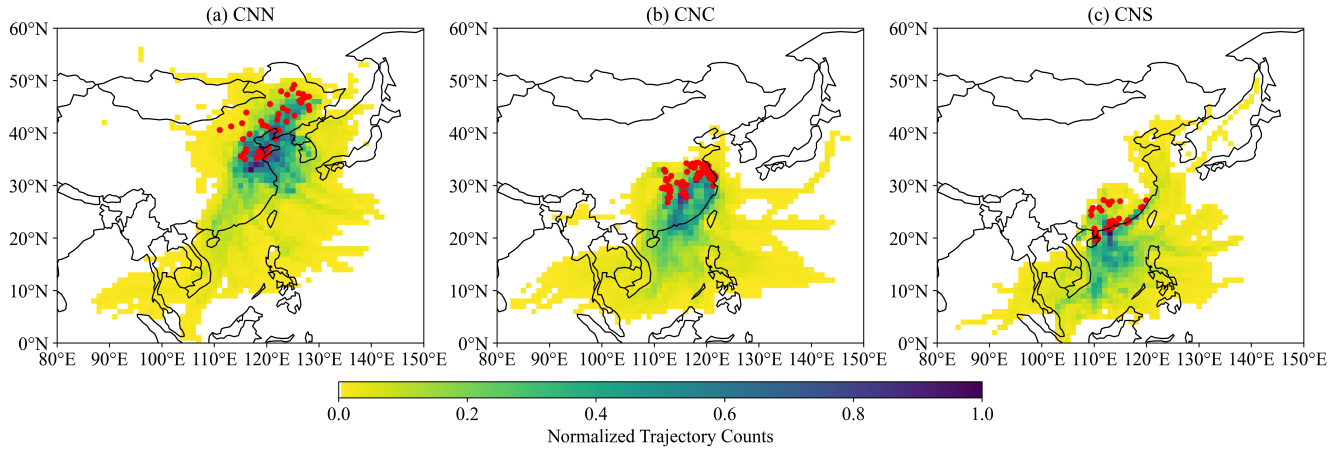

Figure 1. Backward-trajectory counts normalized by the total number of trajectories for air parcels for tornadoes in each of the (a) CNN, (b) CNC, and (c) CNS regions. Red dots denote tornado locations.

To provide a more detailed analysis of the proportions of moist inflow air that feed tornadoes in different regions, the geographical area spanning 0°N to 60°N and 80°E to 150°E is divided into 10 subregions (Figure 2a). These subregions include the land areas of North Asia (NA), northern China (CNN), central China (CNC), southern China (CNS), and Indochina (IDC), as well as the mostly maritime regions of the Bay of Bengal (BOB), the South China Sea (SCS), the East China Sea (ECS), the northern part of the western North Pacific (NWNP), and the southern part of the western North Pacific (SWNP). The definition of the ECS also includes the Bohai Sea and the Yellow Sea. Figure 2b shows the proportion of air parcel origins (backward trajectory end points 120 hours earlier) located over the 10 sectors for tornadoes in CNN, CNC, and CNS. For tornadoes in CNN, a considerable proportion of 22.9% of air parcels originate from the CNN land region.

Compared to tornadoes in other regions, the land-origin proportion for tornadoes in CNN is notably larger at 44.3%. The East China Sea, the South China Sea and the northern part of the western North Pacific are also key origins of air parcels, contributing 18.7%, 14.0% and 13.3%, respectively. Additionally, more than 80% of air parcels for tornadoes in CNC and CNS originate from maritime regions, with the South China Sea contributing the largest share. Especially for tornadoes in CNC, 53.9% of air parcels originate from the South China Sea. Both of them have approximately 10% of air parcels originating from the Bay of Bengal. More air parcel origins are located over the southern part of the western North Pacific for tornadoes in CNS compared to CNC (14.3%; 11.5%). Overall, tornadoes in the CNN region are often strongly influenced by nearby land. In contrast, the tornadoes in the CNC and CNS regions experience longer-range air parcel transport, where the air parcels typically travel greater distances before reaching these areas.

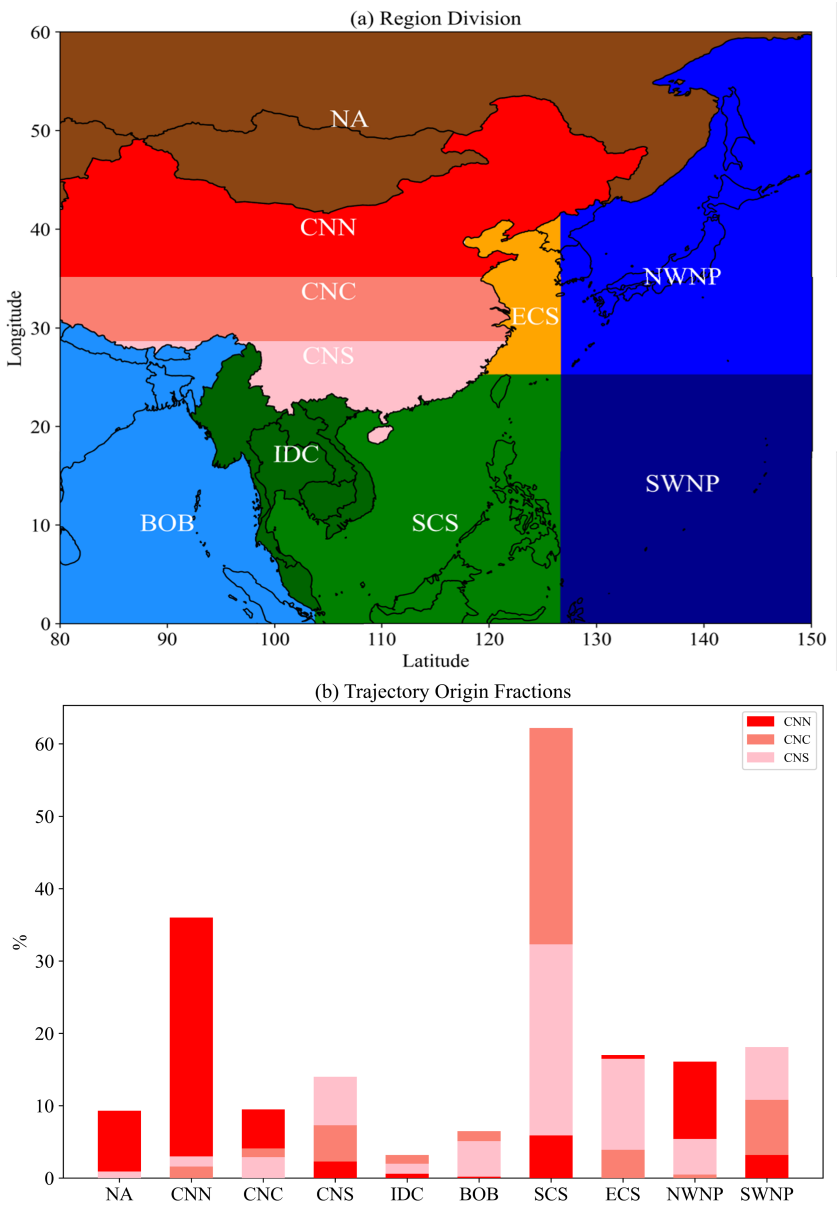

Figure 2. (a) 10 regional divisions include North Asia (NA), northern China (CNN), central China (CNC), southern China (CNS), Indochina (IDC), the Bay of Bengal (BOB), the

South China Sea (SCS), the East China Sea (ECS), the northern part of the western North Pacific (NWNP), and the southern part of the western North Pacific (SWNP). (b) Proportion of trajectory origins in 10 sectors for tornadoes in CNN, CNC, and CNS regions.

4. Trajectory clustering

4.1 Cluster numbers with *k*-means for the subregions

The same type of meteorological event often has different moisture transport pathways. Cheng et al. (2021) disentangled 15 dominant moisture channels along four corridors reaching the Somali Jet, South Asia, Bay of Bengal, and Pacific basin for the warm-season rain belts in East Asia. Huang et al. (2018) found five characteristic trajectories and corresponding circulation patterns of moisture transport for wintertime extreme precipitation events over South China. Here, we use *k*-means clustering to classify trajectories for tornadoes in CNN, CNC, and CNS separately.

A cluster number of 3, 3, and 4 is selected for tornadoes in CNN, CNC, and CNS, respectively, representing distinct moisture channels originating from different oceanic or terrestrial sources.

4.2 Moisture channels for tornadoes in the CNN region

The average trajectory and average specific humidity along all trajectories in each cluster or moisture channel are shown in Figure 3 for tornadoes in the three subregions. The mean specific humidity and relative humidity at tornado locations for each channel are displayed in the upper left corner. The text in the bottom right corner indicates the frequency of occurrences for each channel. For tornadoes in CNN (top row in Figure 3), the N_ECS and N_CNN are two predominant tornado moisture channels, accounting for about 58.7% and 34.8% of total trajectories in the CNN region (Figures 3a and 3b). Their corresponding tornado locations exhibit lower specific humidity. This is consistent with the lower humidity characteristic observed in the average tornado environment in CNN (Zhang et al., 2023). The N_ECS channel (Figure 3a) originates over the East China Sea. It then travels across Shandong Province, continuing northward and passing through the Bohai Sea. Another important moisture channel named N_CNN (Figure 3b) starts in the CNN region and moves southward towards the Yellow Sea, where it then curves clockwise and returns to the CNN region again. The NCN channel provides the least favorable moisture conditions for CNN tornadoes ($q = 11.7g\ kg^{-1}$; Figure 3b).

Tornadoes in CNN also receive moisture transported from the relatively remote South China Sea (N_SCS, Figure 3c). The N_SCS only accounts for about 6.5% of all moisture channels in the CNN region. The relatively low frequency underscores the status of N_SCS as a rare pathway. This least popular moisture transport pathway, starts over the South China Sea and moves northwestward before reaching the CNS region. Upon arrival in CNS, it shifts direction to northeastward and continues across the CNS and CNC regions, finally entering the CNN region. Despite its relatively lower occurrence frequency, this pathway contributes to the complexity of moisture sources affecting tornado formation in CNN. Interestingly, the longest N_SCS channel has the lowest average relative humidity. This phenomenon may be related to the fact that the tornado locations in this channel are the southernmost among all tornadoes in CNN, where the temperature tends to be higher.

4.3 Moisture channels for tornadoes in the CNC region

The main moisture channel for tornadoes in CNC (middle row in Figure 3) originates from the South China Sea, identified as C_SCS (Figure 3d). C_SCS contributes to 79.8% of all moisture trajectories in the CNC region. In this channel, air parcels from the South China Sea move northward, first entering the CNS region and then veering northeastward to reach the CNC region.

There are two atypical moisture transport channels, C_SWNP and C_BOB, each occurring with a frequency of approximately 10.1%. The C_SWNP channel originates over the southern part of the western North Pacific (Figure 3e). As the channel moves across the ocean, it follows a northwestward direction before reaching the land. Another distant moisture channel, C_BOB (Figure 3f), exhibits a similar occurrence frequency to C_SWNP. This pathway originates from the Bay of Bengal and follows a predominantly northeast route. As it progresses, it traverses through Indochina, the South China Sea, and CNS before eventually reaching the target region, highlighting the influence of remote moisture origins on tornadoes within CNC.

4.4 Moisture channels for tornadoes in the CNS region

The trajectories for the moisture channels for tornadoes in the CNS region are plotted in the bottom row of Figure 3. The South China Sea serves as an important origin of air parcels for tornadoes in CNS, with the S_SCS channel (Figure 3g), which accounts for about 63.8%. Over the sea, S_SCS follows a curve, transitioning from a westward direction to a more southward trajectory before eventually reaching land.

There are three unusual moisture transport channels (S_SWNP, S_ECS and S_BOB) in the CNS region, with frequencies of approximately 14.9%, 12.8%, and 8.5%, respectively. The moisture channel originating from the southern part of the western North Pacific (S_SWNP, Figure 3h) follows a similar trajectory to that of C_SWNP. Additionally, there is a unique channel called S_ECS (Figure 3i), which originates in the northern East China Sea and continues to flow toward the CNS region along the eastern coastline. The S_BOB pathway (Figure 3j) originates in the Bay of Bengal, traverses the western part of the Malay Peninsula, then crosses the Gulf of Thailand, and continues through the Indochina Peninsula and the South China Sea.

5. Moisture uptake

5.1 Characteristics of moisture sources for tornadoes in three subregions

Figure 4 shows the box-and-whisker graphs of MU (moisture contribution) proportion across 10 subregions defined in Figure 2a for tornado cases in (a) CNN, (b) CNC and (c) CNS regions. The lower whisker extends to the 5th percentile, and the upper whisker extends to the 95th percentile. The dot and horizontal line within each box represent the mean and median, respectively, calculated from the data between the lower and upper whiskers. The upper quartile corresponds to the 75th percentile and the lower quartile corresponds to the 25th percentile. For tornadoes in CNN (Figure 4a), most moisture contributions are from terrestrial subregions. The largest moisture contribution is from the CNN region, ranging from 1.3% to 80.8% with a mean value of 27.2%. This indicates that tornadoes in CNN exhibit an important moisture recycling process. Another key contributor is the East China Sea, with an average contribution of 22.1%. The third largest moisture source contribution comes from CNC (~21%). Despite having a mean

value of 4.4%, the northern part of the western North Pacific is still a relatively important contributor, particularly when compared to other subregions, whose contributions are less than 2%.

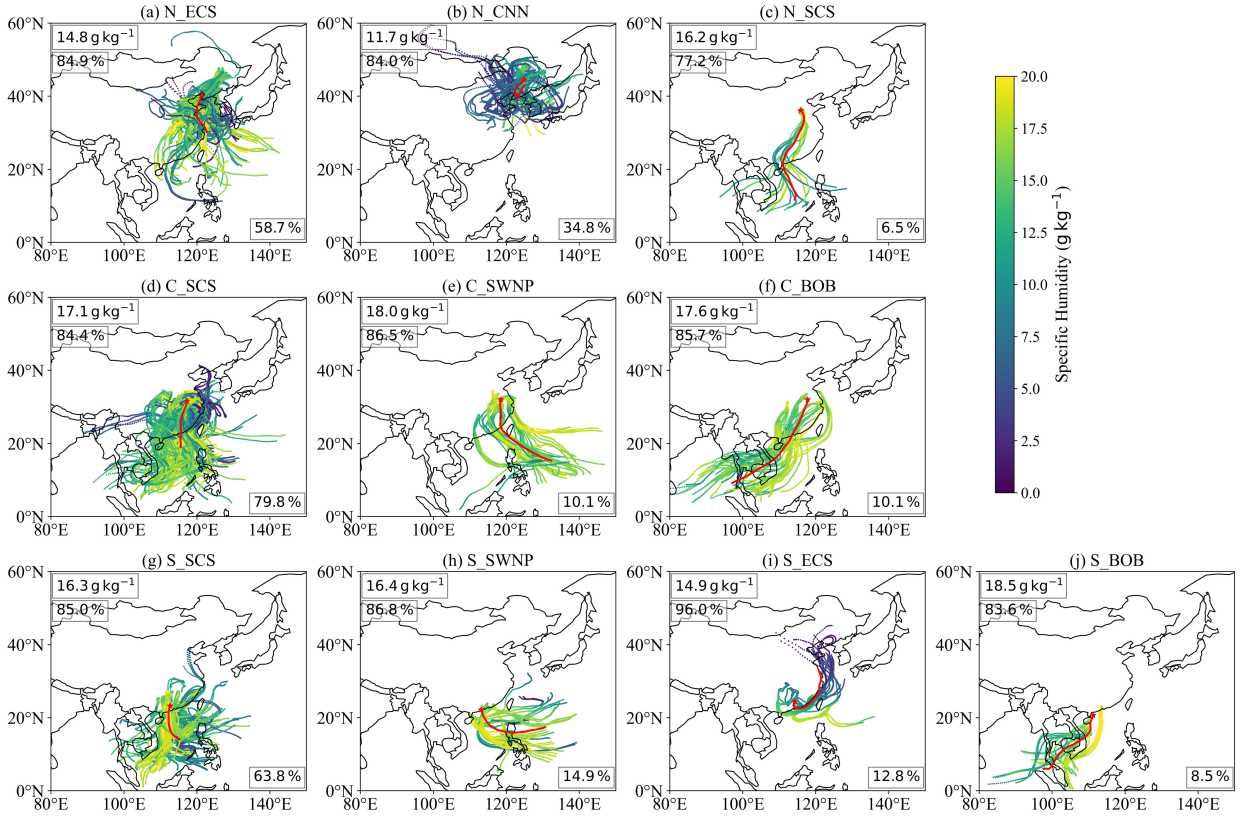

Figure 3. Specific humidity along the trajectories in each moisture channel identified by the *k*-means clustering algorithm. The top row contains 3 channels for the CNN tornadoes, middle row is for 3 channels for CNC tornados and the bottom two rows containing 4 channels are for tornadoes in CNS. Only 1 in every 20 trajectories is plotted. The mean specific humidity and relative humidity of tornado locations for each channel are displayed in the upper left corner. The text in the bottom right corner indicates the frequency of occurrences for each channel.

Although most of the air parcels (120 hours earlier) are from the South China Sea (Figure 2b), tornadoes in CNC (Figure 4b) have their largest moisture uptake contributions from moisture recycling (i.e., from the CNC region itself), with an average value of 51.0%. The CNS region is another important terrestrial contributor (~10%). The South China Sea stands as the primary maritime contributor with an average value of 25.0%. In addition, a smaller fraction of the moisture sources is from the East China Sea, with contributions varying between 0% and 25.7%

Compared to tornadoes in the CNN and CNC regions, where terrestrial moisture sources dominate, the moisture sources of tornadoes in the CNS region exhibit a distinct pattern, with a substantial majority of moisture contributions coming from maritime sources. For tornadoes occurring in the CNS region, as illustrated in Figure 4c, remarkable moisture comes from maritime subregions. The South China Sea stands out as a significant contributor, accounting for a mean value of 71.3%, with its influence ranging from 21.1% to as much as ~100%, highlighting the

dominant role of the South China Sea in supplying moisture for tornadoes in the CNS region. Moisture recycling, or the moisture contribution from the CNS region itself, ranks as the second largest contributor, with an average value of 13.0%. However, this is much lower than the contributions from the South China Sea.

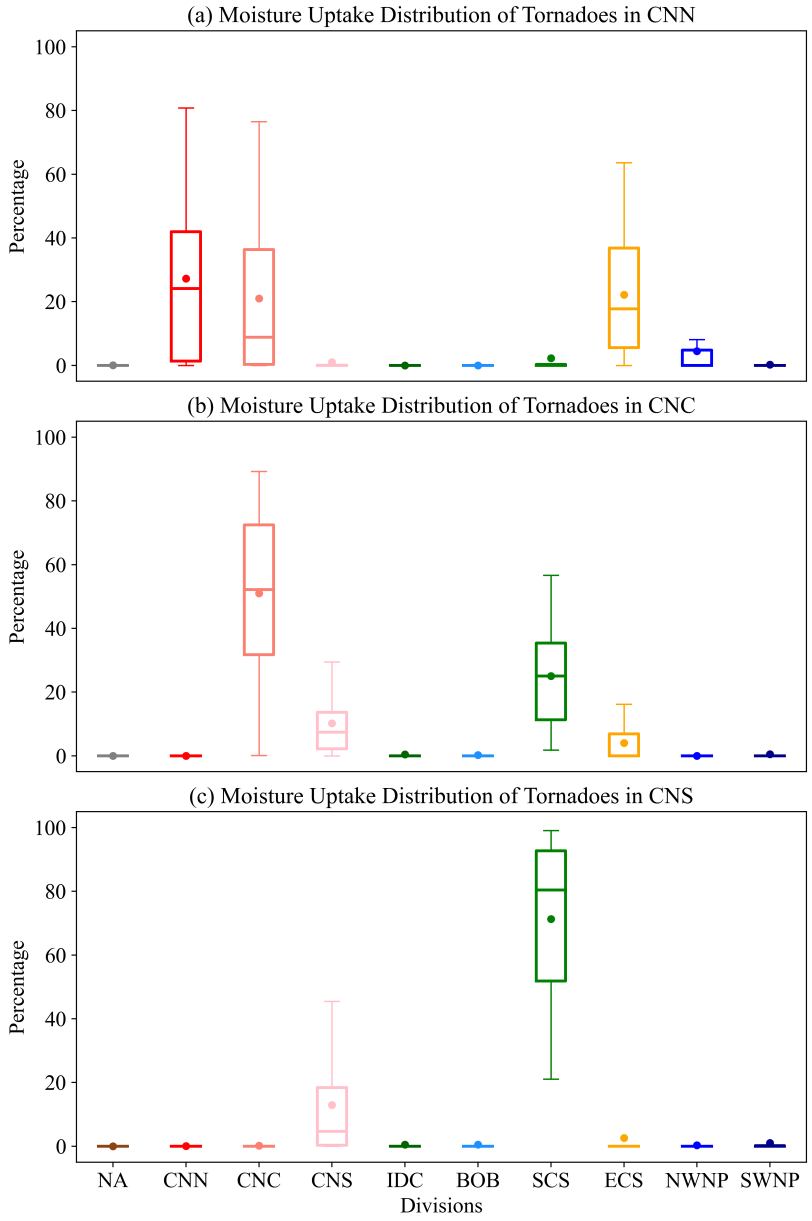

Figure 4. Box-and-whisker graph of the moisture uptake proportion across 10 divisions described in Figure 2a for (a) tornadoes in CNN, (b) tornadoes in CNC, and (c) tornadoes in CNS.

5.2 Characteristics of moisture sources for moisture channels associated with CNN tornadoes

Figure 5 presents the MU contribution proportions of each moisture channel in the subregions defined in Figure 2a. Figure 6 shows the vertical cross sections of the MU values normalized by

their maximum for each moisture channel. The *x*-axis represents the distance from tornado events to MU locations. It is noteworthy that part of the MU is found below 250 m above ground level (Figure 6). At such low levels, the HYSPLIT trajectories may involve larger uncertainties, as turbulence is stronger in the lowest boundary layer. Nevertheless, the main results are not substantially affected by this limitation. Regarding the most popular channel of CNN tornadoes, which is characterized by travel over the East China Sea, N_ECS (Figure 3a), collects a larger proportion of MU values from the East China Sea (29%; Figure 5a). The largest terrestrial contributor is the CNC region at 34.1%, followed by moisture recycling (i.e., the CNN region), which accounts for 25.1%. This channel has surficial sources at a distance of 500 km (Figure 6a). This closer surface maximum source suggests that tornadoes associated with N_ECS primarily draw water vapor evaporated from the surface of the Bohai Sea.

In addition, more than half of the moisture sources carried by the N_CNN moisture channel (Figure 3b) are from the CNN region (Figure 5b). As another common moisture channel for CNN tornadoes, N_CNN differs from N_ECS in that, in addition to sourcing 30.0% from the East China Sea, it also obtains 12% from the northern part of the western North Pacific (Figure 5b). Apart from a considerable proportion of MU values lying at the surface within a distance of 500 km to 1000 km, peak MU values are observed within a horizontal distance of 500 km, and they are characterized by elevated moisture sources located at a height between 250 m and 500 m (Figure 6b). MU values that occur at the surface are typically linked to soil moisture evaporation and vegetation evapotranspiration processes. However, for elevated MU values that occur above the surface (but at or below the HPBL), Molina and Allen (2019) discussed several possibilities. The possible reasons include: (i) air parcels interacting with buoyant air masses rising from below due to unstable thermodynamic vertical profiles extending above the HPBL, (ii) travel across cloud condensation, (iii) topographic errors related to the Rockies or the Caribbean (in their study), and (iv) precipitation falling along air parcel trajectories.

The longest channel, N_SCS (Figure 3c), transports 29.5% of moisture from the South China Sea and 62.1% from CNC (Figure 5c). The N_SCS channel sources peak moisture from nearby locations (< 500 km), and from elevated areas (Figure 6c), which may be associated with precipitation in this region.

5.3 Characteristics of moisture sources for moisture channels associated with CNC tornadoes

The popular moisture channel for CNC tornadoes, C_SCS channel (Figure 3d), draws significantly moisture sources from the CNC region, accounting for 53.2%. The South China Sea plays a secondary role in contributing 25% moisture for the C_SCS channel. In addition, the C_SCS channel also gains 14.4% moisture from the CNS region. The vertical cross-section of normalized MU for this channel reveals that most moisture sources are from nearby elevated regions (Figure 6d).

Nearly half of the moisture sources transported by the easternmost C_SWNP channel (Figure 3e) come from the CNC region (Figure 5e). This is consistent with the vertical cross-section of normalized MU for the CSW channel, which shows peak MU values occurring within 500 km above the surface (Figure 6e). Two additional maritime subregions mainly contribute to the remaining portions of moisture sources. They are the South China Sea (24.4%) and the southern portion of the western North Pacific (12.7%). The C_BOB channel originating from the Bay of

Bengal (Figure 3f) exhibits the most diverse source regions (Figure 5f). This channel collects 40.6% of moisture sources from the South China Sea, with another substantial contribution of 34.0% from the CNC region. Notably, it carries 7.4% and 7.5% of moisture sources from the Bay of Bengal and Indochina, respectively—regions that rarely contribute to other moisture channels. The C_BOB channel is the only channel that carries more sources from the maritime area than the terrestrial area among moisture channels reaching the CNC region. Additionally, the vertical cross-section for the C_BOB channel reveals that the peak MU values are elevated and occur within a 100 km horizontal range (Figure 6f).

5.4 Characteristics of moisture sources for moisture channels associated with CNS tornadoes

The S_SCS moisture channel (Figure 3g) gains the majority of its moisture sources from the South China Sea, with proportions of 76.6% (Figure 5g). The remaining moisture primarily comes from the CNS region (19.5%). This channel mainly draws moisture sources from the surface (Figure 6g).

The S_SWNP, originating from the southern part of the western North Pacific (Figure 3h), has 17.4% of the moisture sources coming from this region (Figure 5h). A significant 77.0% of moisture sources originate from the South China Sea, which is a major contributor to tornadoes in the CNS region. Most sources from these subregions are found both elevated and at the surface (Figure 6h). The moisture contribution brought by the S_ECS channel (Figure 3i) is almost evenly distributed among the South China Sea, the East China Sea, and CNS regions (34.3%, 30.7% and 28.1%; Figure 5i). The S_ECS channel carries most moisture sources from the nearby surface (Figure 6i). The S_BOB channel originating from the westernmost position (Figure 3j) also carries more than half of the moisture (56.5%) from the South China Sea and some moisture from the Bay of Bengal and Indochina (11.0% and 15.3%; Figure 5j). It initially draws moisture from surface sources, but as it approaches the tornado sites, it primarily pulls from elevated sources (Figure 6j).

6. Synoptic-scale circulation patterns

6.1 Circulations for moisture channels associated with CNN tornadoes

Tornado events in the CNS region predominantly occur during the spring season (approximately 77%). As the season shifts from spring to summer, enhanced continent-ocean thermal contrast strengthens the southwest monsoon flows, while the warming of the western Pacific favors the intensification and westward extension of the western North Pacific subtropical high (WNPSH). These two large-scale circulation systems together drive strong southerly winds, which in turn facilitate substantial northward transport of moisture. As the main precipitation regions shift from south China in the spring to the Yangtze River region, then north China from early through late summer, most frequent occurrences of tornadoes also shift northward. This deeper northward advancement of moisture contributes to the increased frequency of tornado occurrences in the CNC and CNN regions, where around 83% and 75% of tornadoes occur during the summer, respectively. To identify the critical synoptic-scale circulation patterns responsible for boundary-layer moisture transport for tornadoes in the CNN, CNC, and CNS regions, we perform a time evolution analysis of composite circulation for each moisture channel (Figures 7-12). This analysis focuses on the 850-hPa layer, which aligns with most trajectories and avoids much of the orographic blockage. There may be mismatches between the MU heights and the 850-

hPa layer, but our focus is on the circulation patterns that primarily govern the trajectories, which are not strictly confined below 1 km and may extend to much higher altitudes during the five-day backward tracking period. Since tornadoes in different regions exhibit different seasonal tendencies, the 850-hPa geopotential height anomalies are calculated as the mean deviations of daily fields from the corresponding seasonal-mean daily climatology [spring (3-5 months) for tornadoes in CNS, and summer (6-8 months) for tornadoes in CNN and CNC] for the period from 1980 to 2021. This approach aims to identify the anomalous systems that differentiate tornado-forming periods from non-tornado periods within the tornado-prone season.

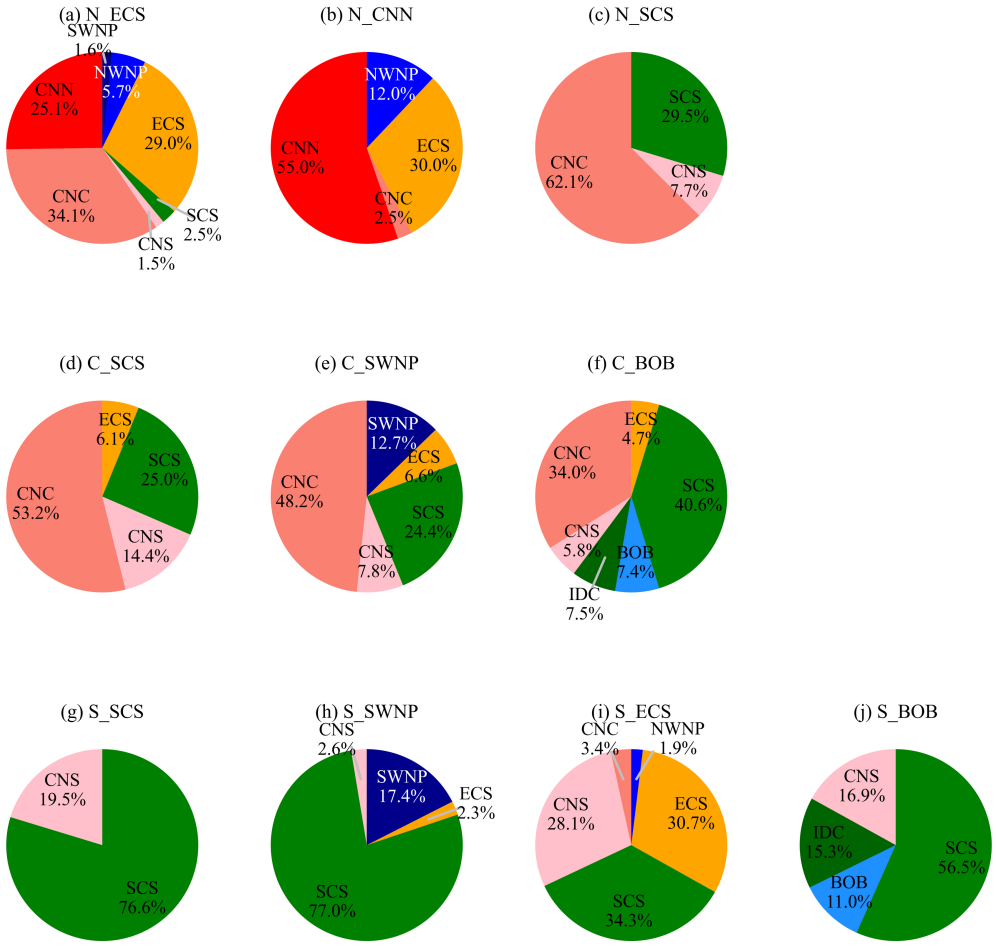

Figure 5. Pie charts of the MU contributions from 10 divisions assigned to each tornado moisture channel. The top row contains MU proportions of 3 channels for the CNN tornadoes, the middle row is for MU proportions of 3 channels for CNC tornadoes and the bottom row contains MU proportions of 4 channels for tornadoes in CNS. Only moisture uptake contributions greater than or equal to 1% are shown.

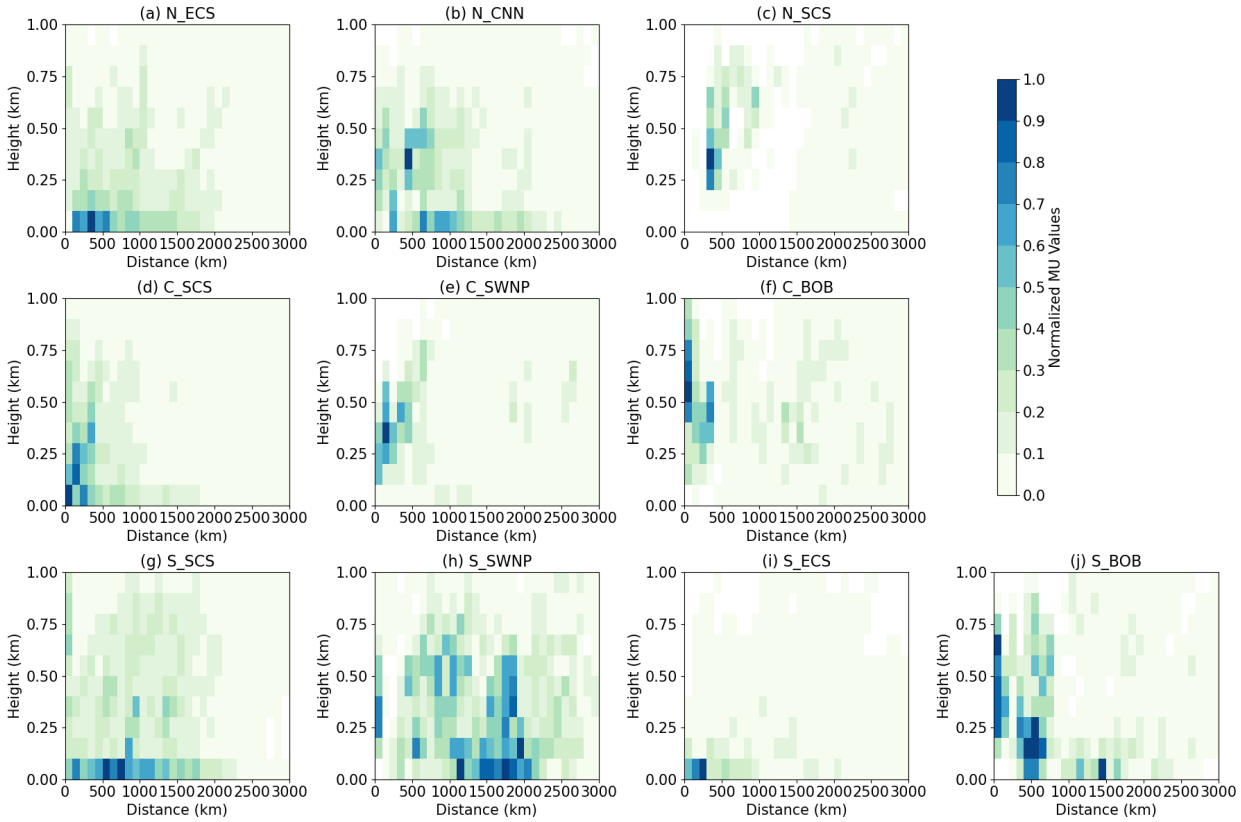

Figure 6. Vertical cross sections of normalized MU values for moisture channels. The top row contains vertical cross sections of 3 channels for the CNN tornadoes, the second row is for vertical cross sections of 5 channels for CNC tornadoes and the last row contains vertical cross sections of 4 channels for tornadoes in CNS. Heights are above ground level.

One of the most common synoptic-scale patterns associated with CNN tornadoes is the cyclone-anticyclone coupling within the N_ECS channel. In this pattern, a northerly wind over East China Sea (~30°N) initially governs the early transport of moisture in the N_ECS channel (Figures 7a and 7b). In the later stage, the combined influence of a northern low-pressure system and a southern high-pressure system facilitate the N_ECS transport (Figures 7c and 7d).

Another prominent pattern in the CNN region associated with CNN tornadoes (the N_CNN channel) involves the influence of a northern low-pressure system in China. On day -5, a northern low situated over the N_CNN moisture channel effectively blocks the southwest flow from reaching the target region (Figure 7e). This system forces the moist air southward, pushing it over the nearby sea (Figure 7f). By day -3, the moist air over the sea is positioned between the north low and the advancing southwest flow. Under the influence of the southward-moving north low, this moist air is gradually funneled back toward the tornado locations (Figures 7g and 7h). The north-low pattern of the N_CNN channel resembles the cold vortex-type tornadoes in China (Zheng 2020). Yuan et al. (2023) analyzed the environmental characteristics of tornadoes in Liaoning Province and found that 87% were associated with cold vortex systems. Their conceptual model for tornadoes under typical synoptic conditions suggests that moist air is transported from the Bohai Sea to the tornado locations. Building upon this, our study uses Lagrangian trajectories to track moist air over 5 days (from day -5 to day 0) and found that tornadoes under such a north-

low pattern typically draw air from the local region, which moves southward toward the Bohai Sea and subsequently travels back toward the tornado locations, consistent with the findings of Yuan et al. (2023) regarding the final stage of moisture transport.

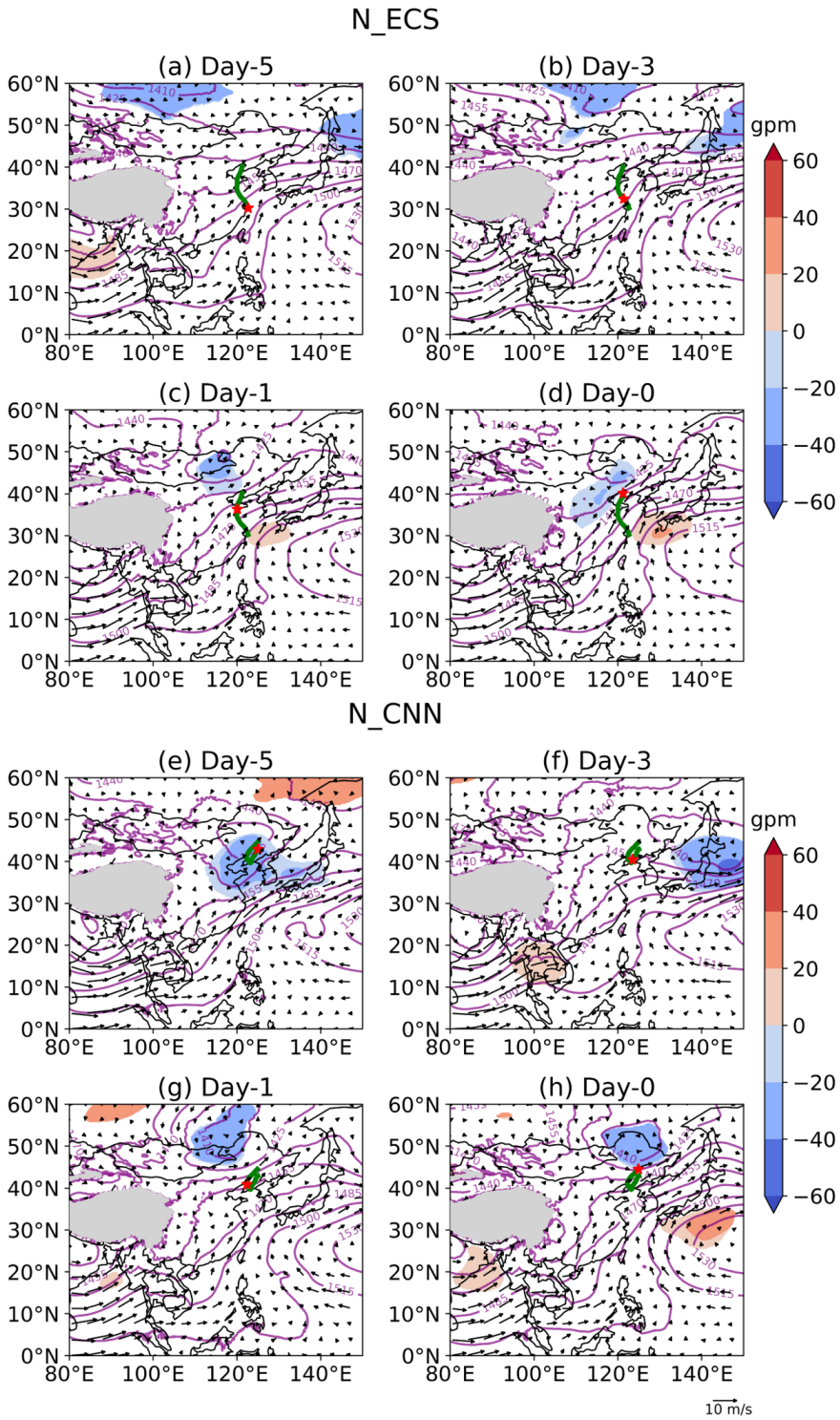

Figure 7. Time evolution of the composite 850-hPa geopotential height (purple lines; unit: gpm), geopotential height anomalies (shaded; unit: gpm) and horizontal wind (vectors; unit: m/s) for the N_ECS (a–d) and N_CNN (e–h) moisture channels. Day-0 marks the onset of the event. Shading is displayed only where the anomalies reach the 95% confidence level, based on a two-tailed Student's *t*-test. The red star marks the location of the moisture channel at the corresponding time and the green line denotes the average trajectory of the moisture channel.

In addition to the north low-south high coupling patterns and the northern low-pressure system, we also identify a less common pattern for tornadoes in the CNN region. The pattern of the N_SCS moisture channel is characterized by the westward extension of the western North Pacific subtropical high (WNPSH; approximately 25-40°N). On Day -5, there is an anomalous southwest monsoon and an anomalous cyclone over the South China Sea, both of which facilitate the transport of moist air over the region (Figure 8a). Additionally, from Day -5 to Day -0, the WNPSH expands westward and strengthens, effectively controlling the N_SCS moisture channel and directing its transport along the eastern circulation of WNPSH (Figures 8a-8d). By Day -1, a low-pressure anomaly appears over the eastern side of the Tibetan Plateau, subsequently expanding eastward with anomalous values exceeding 40 gpm (Figures 8c and 8d). This low-pressure system also plays a critical role in the final stage of moisture transport with the N_SCS channel for tornadoes in CNN.

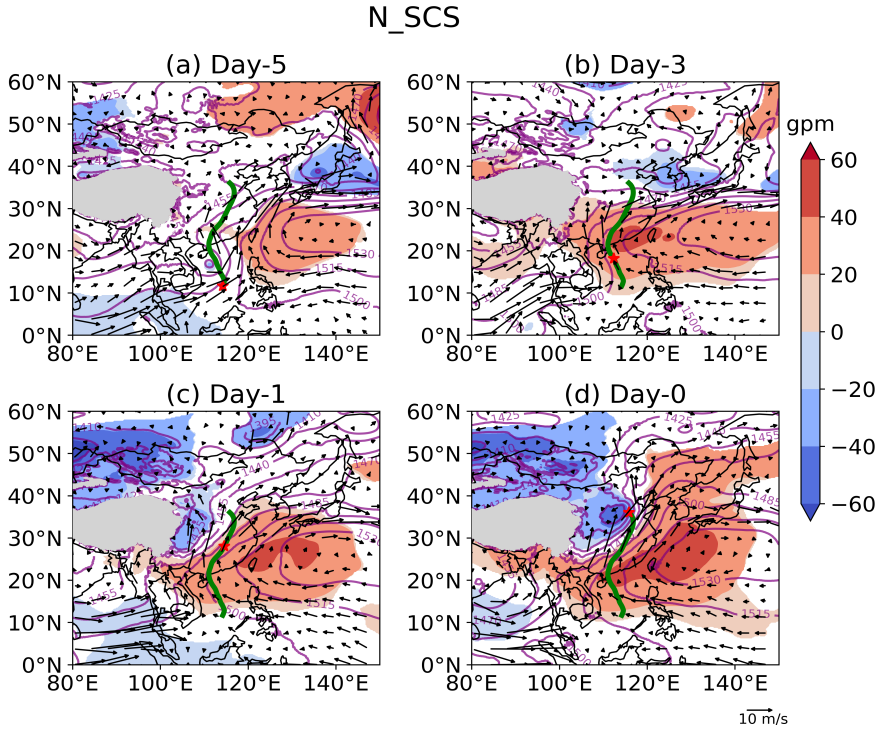

Figure 8. As in Figure 7, but for N_SCS moisture channel.

6.2 Circulations for moisture channels associated with CNC tornadoes

The synoptic-scale patterns that govern moisture channels for tornadoes in CNC are closely linked to the activity of WNPSH, the southwest monsoon flows, and the mid-latitude low-pressure system. When the WNPSH is unusually strong, its dominant circulation steers the primary moisture channels toward CNC, facilitating the moisture needed for tornado formation. In contrast, during periods when the WNPSH weakens or decays, the southwest monsoon flows originating from the Bay of Bengal and the mid-latitude low-pressure system located approximately 30-60°N become the primary drivers of moisture transport into the region.

Following a pattern similar to the N_SCS channel (Figures 8a-8d), the C_SCS channel (the most popular channel for tornadoes in CNC) also benefits from the westward extension of the WNPSH and the eastward expansion of a mid-latitude low-pressure anomaly (Figures 9a-9d). Due to the relatively limited extent of the WNPSH anomaly, the moisture transport channel is confined to a shorter path.

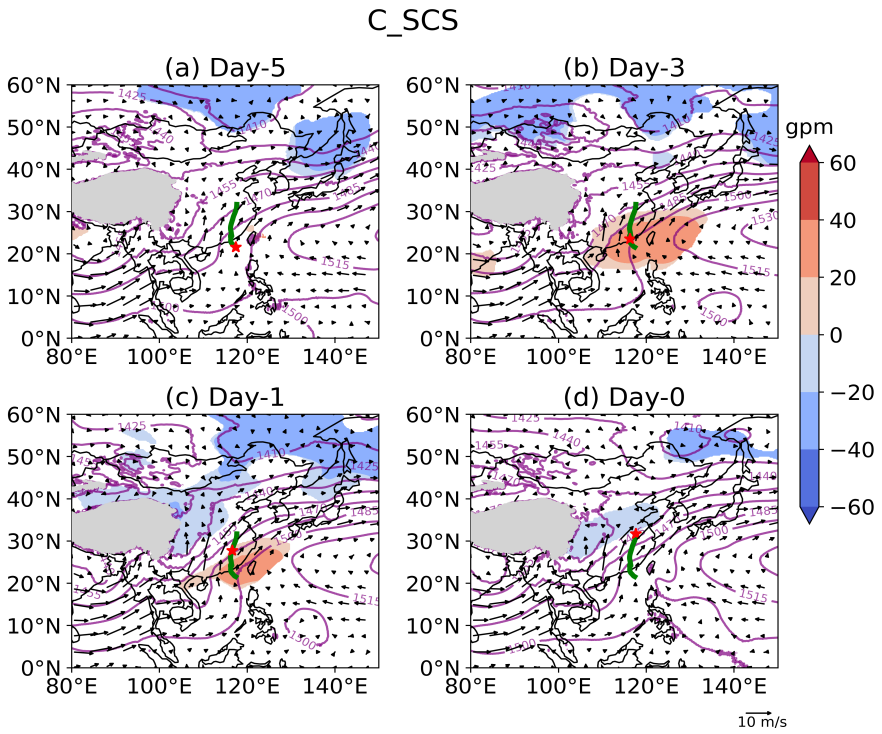

Figure 9. As in Figure 7, but for C_SCS moisture channel.

Most of the moisture channels for tornadoes in the CNC region are controlled by the westward-moving WNPSH, while a small portion of the moisture channels (C_SWNP and C_BOB) are influenced by other anomalously moving WNPSH or the southwest monsoon. The moisture transport pattern for the C_SWNP channel is primarily controlled by the anomalously strong northward extension of the WNPSH (Figures 10a-10d). The WNPSH gradually intensifies and shifts northward from Day -5 to Day 0, effectively transporting moist air from distant oceanic regions to the target area. Meanwhile, starting on Day -3, the strong southwesterly monsoon flows also contribute to moisture transport, playing a complementary role in this process. Another

channel pattern, C_BOB, is observed under a weakened WNPSH, where the moisture channel primarily follows the monsoon flow direction (Figures 10e and 10f). As the moist air reaches around 25°N over land, it is further influenced by the southward extension of a low-pressure system, which helps guide the moisture transport (Figures 10g and 10h).

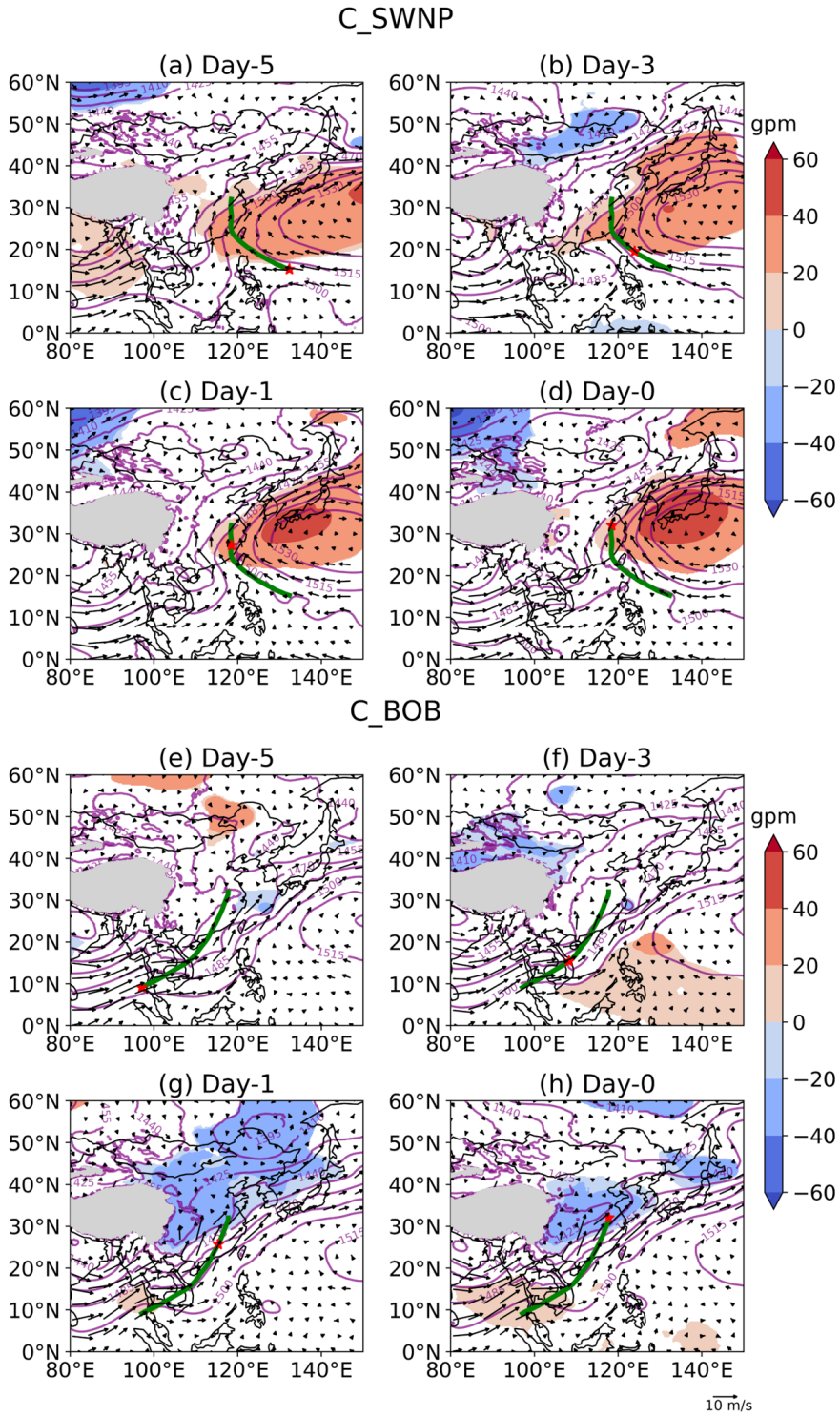

Figure 10. As in Figure 7, but for C_SWNP (a-d) and C_BOB (e-h) moisture channels.

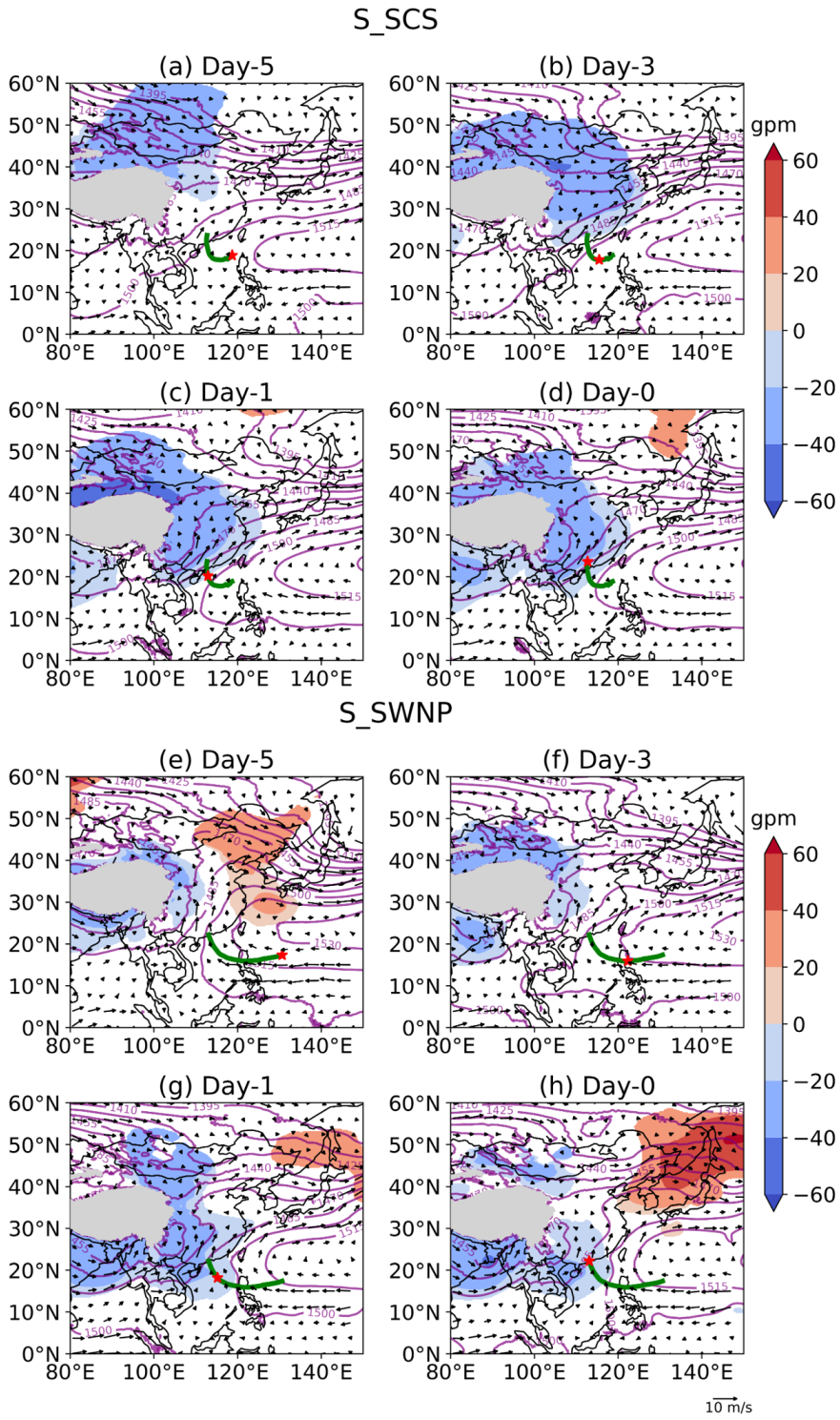

Figure 11. As in Figure 7, but for S_SCS (a-d) and S_SWNP (e-h) moisture channels.

6.3 Circulations for moisture channels associated with CNS tornadoes

In spring, when many of the CNS tornadoes form, abundant moisture is transported from the ocean to the CNS region, providing the necessary conditions for tornado formation. The popular channel named S_SCS associated with CNS tornadoes is influenced by the westward-extending and weakened WNPSH governs the S_SCS channel from Day -5 to Day -3 (Figures 11a and 11b). The strong southwesterly winds in the low-pressure system governs the later stage transport (Figures 11c and 11d).

Circulations that govern the unusual channels named S_SWNP, S_ECS and S_BOB are also identified. The S_SWNP channel is influenced by the westward shift of the WNPSH, following a predominantly east-west trajectory (Figure 11e-11h). Then, the eastward-developing low-pressure system controls the channel (Figure 11g and 11h). Unlike other channels originating from southern oceans, the S_ECS moisture channel draws from northern oceans. This channel is primarily influenced by the southward extension of a mid-latitude trough (Figures 12a and 12b). Before Day -3, the trough pushes the S_ECS channel southward to the Taiwan Strait, after which it continues to move due to the westward expansion of the WNPSH (Figures 12c and 12d). When the southwest monsoon flows intensify further, the moisture channel originates from the western side of Indochina (S_BOB; Figures 12e-12h), rather than the South China Sea (S_SCS; Figures 11a-11d). The low-pressure system also serves as a key contributor to this channel.

7. Summary and conclusions

This study uses the HYSPLIT model (Stein et al., 2015) and a Lagrangian-based algorithm (Sodemann et al., 2008) to investigate moisture sources and transport pathways for spring and summer tornadoes in the CNN, CNC, and CNS regions over the period from 1980 to 2021. The ERA5 data are used to drive the HYSPLIT model and produce time-evolving composite circulation analyses. The backward trajectories reveal that tornadoes in the CNN region are primarily influenced by air parcels originating nearby. In contrast, tornadoes in the CNC and CNS regions are characterized by long-range air parcel transport, with air masses typically traveling greater distances before reaching the target areas. The *k*-means clustering method (Wilks, 2011) is applied to classify the trajectories of the three regions, resulting in the identification of ten moisture channels (3 for CNN, 3 for CNC and 4 for CNS tornadoes) originating from the CNN region, East China Sea, southern part of the western North Pacific, South China Sea, and Bay of Bengal. Apart from the prominent N_ECS and N_CNN channels, the less common N_SCS channel also contributes moisture to tornadoes in the CNN region. C_SCS is recognized as the primary channel for transporting moisture to the CNC region, while other unusual channels for tornadoes in the CNC region include C_SWNP and C_BOB. For tornadoes in the CNS region, S_SCS is a frequently observed channel, along with less popular channels identified as S_SWNP, S_ECS, and S_BOB (see Figure 3 for the definitions of these moisture channels).

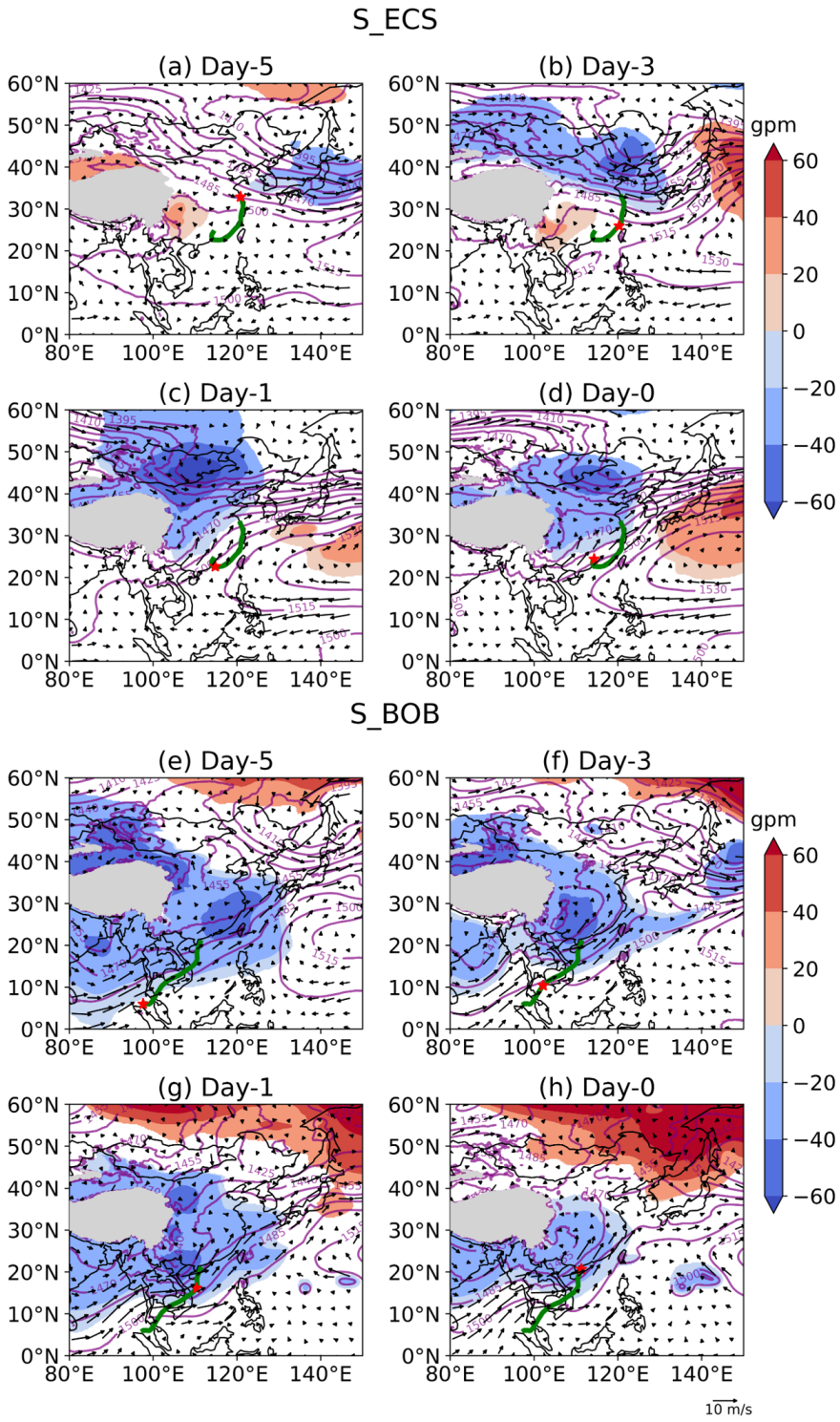

Figure 12. As in Figure 7, but for S_ECS (a-d) and S_BOB (e-h) moisture channels.

The Lagrangian analyses show distinct characteristics of moisture sources for tornadoes in the CNN, CNC, and CNS regions. For tornadoes in CNN and CNC, the primary moisture contributions or uptake along the trajectories come from terrestrial sources, while for tornadoes in CNS,

maritime sources dominate. Moisture contributions for tornadoes in each region are concentrated within a few key subregions. For CNN tornadoes, the contributions primarily come from four areas: the CNN region itself (~27.2%), the East China Sea (~22.1%), the CNC region (~21.0%), and the northern part of the western North Pacific (~4.4%). Specifically, the N_ECS channel primarily collects moisture uniformly from the CNC region, with a substantial contribution from the East China Sea as well as the CNN region. Besides, most moisture sources in N_ECS are at the surface. The N_CNN moisture channel is predominantly sourced from the CNN region, with important contributions from the East China Sea and the northern part of the western North Pacific. The N_CNN channel mainly draws elevated sources. The infrequent N_SCS channel sources moisture mainly from the CNC region and the South China Sea. In addition, this channel primarily draws moisture from elevated sources.

For tornadoes in CNC, the dominant moisture sources are the CNC region (~51.0%), the South China Sea (~25.0%), and the CNS region (~10.2%). The C_SCS channel mainly sources moisture from the CNC region, with significant contributions from the South China Sea and the CNS region. Compared to the C_SCS channel, the less popular C_SWNP channel has additional sources from the southern part of the western North Pacific. Another less frequent C_BOB channel has the most diverse sources, primarily taking moisture from the South China Sea and CNC region, and is unique in having more maritime contributions than terrestrial ones. All three channels draw their peak moisture from elevated sources.

Tornadoes in the CNS region rely heavily on just two subregions: the South China Sea (71.3%) and the CNS region itself (13.0%). A total of 4 channels is identified by the *k*-means clustering for CNS tornadoes. The most popular channel named S_SCS draws most of its moisture sources from the South China Sea, and the CNS region also provides a minor contribution of moisture. In addition to drawing abundant moisture from the South China Sea, the rare S_SWNP channel also collects moisture from the southern western North Pacific. The special S_SEC channel, which transports moisture southward to the CNS region, consistently gathers moisture from the South China Sea, the East China Sea, and the CNS region. The infrequent S_BOB channel collects a significant amount of moisture from the South China Sea, with additional contributions from the CNS region, Indochina, and the Bay of Bengal. The S_SCS and S_ECS channels mainly draw moisture from the surface, whereas the S_SWNP and S_BOB channels also receive contributions from elevated sources.

As demonstrated in this paper, although the moisture channels may supply moisture to the same region, their characteristics can differ significantly. The associated synoptic-scale patterns provide valuable insights into the reasons for these differences. Figure 13 shows the schematic diagram of circulations for moisture channels in different regions. In spring, the WNPSH and the monsoon flows are typically weak (Figure 13c), allowing abundant moisture from the Southern Ocean to reach the nearby CNS region rather than the deeper CNC or CNN regions. Approximately 77% of tornadoes in the CNS region occur during this season. The west-northwest moisture channels (S_SCS and S_SWNP) are affected by the WNPSH but with weaker intensity in spring. During the later transport period, these channels are influenced by an anomalous low-pressure system. When the monsoon flows intensify further, the less common S_BOB moisture channel originates from the western side of Indochina instead of the South China Sea, with the low-pressure system playing a key role. The special S_ECS moisture channel primarily originates from northern

oceans, influenced by the southward extension of a mid-latitude trough and the westward expansion of the WNPSH.

As the seasons transition from spring to summer, the strengthened WNPSH and monsoon flows significantly enhance moisture transport northward. This increased northward moisture transport correlates with a higher frequency of tornado occurrences in the CNC and CNN regions, where approximately 83% and 75% of tornadoes occur during the summer, respectively. In the CNN region, channels are affected by the low-pressure system and the WNPSH (Figure 13a). The N_ECS pattern involves cyclone-anticyclone coupling, where a weakening northern low-pressure system allows the southern high-pressure system to extend northward, facilitating moist air transport. The N_CNN channel is influenced by a north low-pressure system that blocks southwest flow and redirects moist air. The rare N_SCS moisture channel is characterized by the westward expansion of the WNPSH. It is also affected by the mid-latitude low-pressure anomaly in China. Channels in the CNC region are influenced by the monsoon flows (Figure 13b). The most popular C_SCS channel has a similar pattern to the N_SCS channel. The C_SWNP is influenced by the northward extension of the WNPSH. Besides, the C_SCS channel is also affected by a mid-latitude low-pressure system. In a weakened WNPSH state, the CBO channel is more influenced by the southwest monsoon flows and low-pressure systems.

In summary, the circulation patterns associated with tornado moisture channels indicate that when the WNPSH is anomalous, moisture is usually transported to tornadoes through channels originating from the East China Sea, the southern region of the western North Pacific and the South China Sea. In contrast, when under the main influence of the monsoon flows and a low-pressure system over China, moisture channels usually originate from land and the Bay of Bengal.

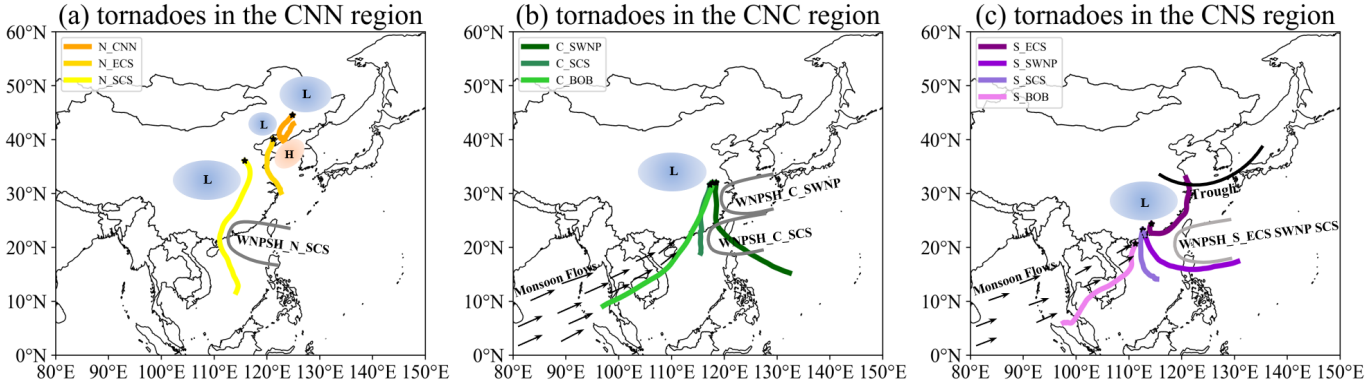

Figure 13. Schematic diagrams illustrating the main characteristics of the circulation patterns for a total of 10 moisture channels related to tornadoes in the (a) CNN, (b) CNC and (c) CNS regions. The L denotes a low-pressure anomaly and H denotes a high-pressure anomaly. The lighter color of WNPSH and less monsoon flows in (c) indicate that the synoptic-scale systems for CNS tornadoes are weaker. The black star denotes the destination of every moisture channel.

We do acknowledge that the sample size of tornadoes in China is small compared to that of tornadoes in the United States although, as mentioned earlier, the general spatial distributions of moisture sources for tornadoes in different regions of China do not change for subsets of tornadoes in years 1980–2001 and 2002–2021. One caveat with the moisture source attributions performed here is the limited spatial resolution of the ERA5 data, and the fact that convective storm

updrafts/downdrafts are not explicitly represented in the data. Trajectories that would otherwise enter the updrafts/downdrafts will not be accurate, but it is hoped that such trajectories comprise only a small fraction of the total number given that updrafts/downdrafts usually occupy a small fraction of total horizontal area. To account for the direct effect of updrafts and downdrafts, convection-resolving simulation or reanalysis datasets will have to be used, which are not currently available. The use of HYSPLIT also has limitations, as noted in the paper. Some air parcels feeding tornadoes in the CNN region are traced back to the cold air behind the front, and part of the moisture sources are located below 250 m above ground level, where turbulence is stronger and HYSPLIT simulations may involve greater uncertainties.

Acknowledgments

This work was primarily supported by NSFC grant 41730965. We thank Prof. Xiaoding Yu for providing the original tornado report database used in this study.

Open Research

The ERA5 reanalysis dataset can be downloaded online (https://cds.climate.copernicus.eu/). The HYSPLIT Model used in this paper can be download online (https://www.arl.noaa.gov/hysplit/). The dataset used in this paper can be accessed at https://doi.org/10.7910/DVN/IC7RLH.

References

Bai, L., Meng, Z., Huang, L., Yan, L., Li, Z., Mai, X., et al. (2017). An integrated damage, visual, and radar analysis of the 2015 Foshan, Guangdong, EF3 tornado in China produced by the landfalling Typhoon Mujigae (2015). *Bulletin of the American Meteorological Society*, **98**(12), 2619–2640. https://doi. org/10.1175/BAMS-D-16-0015.1

Bluestein, H. B. (2013). Tornadoes. In *Severe Convective Storms and Tornadoes* (pp. 307–416). Heidelberg: Springer Berlin.

Brooks, H. E., Doswell, C. A., & Cooper, J. (1994). On the Environments of Tornadic and Nontornadic Mesocyclones. *Weather and Forecasting*, **9**(4), 606–618. https://doi.org/10.1175/1520-0434(1994)009<0606:OTEOTA>2.0.CO;2

Cai, K., Huang, X., Li, C., Yan, L., Li, Z., Gu, B., et al. (2021). Tornado Events and Disaster Characteristics in China in 2020. *Advances in Meteorological Science and Technology*, **11**(1), 40–53. https://doi.org/10.3969/j.issn.2095-1973.2021.01.007

Cai, K., Yu, X., Li, C., Huang, X., Yan, L., He, Q., et al. (2021). Comparative analysis of damage survey of microburst in Lingui of Guangxi and tornado in Zhanjiang of Guangdong in 2019. *Meteorological Monthly*, **47**(2), 230–241. https://doi.org/10.7519/j.issn.1000-0526.2021.02.009

China Meteorological Administration. (2005–2022). *Yearbook of Meteorological Disasters in China*. Beijing: Meteorological Press.

Cheng, T. F., Lu, M., & Dai, L. (2021). Moisture channels and pre-existing weather systems for East Asian rain belts. *npj Climate and Atmospheric Science*, **4**, 32. https://doi.org/10.1038/s41612-021-00187-6

Coffer, B. E., & Parker, M. D. (2015). Impacts of Increasing Low-Level Shear on Supercells during the Early Evening Transition. *Monthly Weather Review*, **143**(5), 1945–1969, https://doi.org/10.1175/MWR-D-14-00328.1.

Ding, Y. (2008). *The collection of meteorological disasters records in China*. Beijing: Meteorological Press.

Edwards, R., Dean, A. R., Thompson, R. L., & Smith, B. T. (2012). Convective modes for significant severe thunderstorms in the contiguous United States. Part III: Tropical cyclone tornadoes. *Weather and Forecasting*, **27**, 1507–1519. https://doi.org/10.1175/WAF-D-11-00117.1

Fan, W., & Yu, X. (2015). Characteristics of spatial-temporal distribution of tornadoes in China. *Meteorology*, **41**(7), 793–805. https://doi.org/10.7519/j.issn.1000-0526.2015.07.001

Fawbush, W., & Miller, R. (1952). A mean sounding representative of the tornadic airmass environment. *Bulletin of the American Meteorological Society,* **33**(7), 303-307. https://doi.org/10.1175/1520-0477-33.7.303

Guo, J., Zhang, J., Shao, J., Chen, T., Bai, K., Sun, Y. et al. (2024). A merged continental planetary boundary layer height dataset based on high-resolution radiosonde measurements, ERA5 reanalysis, and GLDAS. *Earth System Science Data*, **16**(1), 1–14. https://doi.org/10.5194/essd-16-1-2024

Hersbach, H., Bell, B., Berrisford, P., Hirahara, S., Horányi, A., Muñoz Sabater, J., et al. (2020). The ERA5 global reanalysis. *Quarterly Journal of the Royal Meteorological Society*, **146**(730), 1999–2049. https://doi.org/10.1002/qj.3803

Hua, L., Zhong, L., & Ma, Z. (2017). Decadal transition of moisture sources and transport in northwestern China during summer from 1982 to 2010. *Journal of Geophysical Research: Atmospheres*, **122**(6), 12,522–12,540. https://doi.org/10.1002/2017JD027728

Huang, W., He, X., Yang, Z., Qiu, T., Wright, J. S., Wang, B., & Lin, D. (2018). Moisture sources for wintertime extreme precipitation events over South China during 1979–2013. J*ournal of Geophysical Research: Atmospheres*, **123**, 6690–6712. https://doi.org/10.1029/2018JD028485

Huang, X., Yan, L., Cai, K., & Li, Z. (2019). Characteristics of Tornado Activity in China in 2018. *Advances in Meteorological Science and Technology*, **9**(1), 50–55. https://doi.org/ 10.3969/j.issn.2095-1973.2019.01.009

James, P., Stohl, A., Spichtinger, N., Eckhardt, S., & Forster, C. (2004). Climatological aspects of the extreme European rainfall of August 2002 and a trajectory method for estimating the associated evaporative source regions. *Natural Hazards and Earth System Sciences*, **4**(5/6), 733–746. https://doi.org/10.5194/nhess-4-733-2004

Jiang, Z., Jiang, S., Shi, Y., Liu, Z., Li, W., & Li, L. (2017). Impact of moisture source variation on decadal-scale changes of precipitation in North China from 1951 to 2010. *Journal of Geophysical Research: Atmospheres*, **122**(2), 600–613. https://doi.org/10.1002/2016JD025795

Läderach, A., & Sodemann, H. (2016). A revised picture of the atmospheric moisture residence time. *Geophysical Research Letters*, **43**(2), 924–933. https://doi.org/10.1002/2015GL067449

Li, C., Huang, X., Cai, K., Yan, L., & Li, Z. (2018). Characteristics of tornadoes and other convective wind processes, as well as the disaster situation in China in 2019. *Advances in Meteorological Science and Technology*, **10**(1), 7–14. https://doi.org/10.3969/j.issn.2095-1973.2020.01.003

Markowski, P. M., Straka, J. M., & Rasmussen, E. N. (2002). Direct surface thermodynamic observations within the rear-flank downdrafts of nontornadic and tornadic supercells.

Monthly Weather Review, **130**(7), 1692–1721. https://doi.org/10.1175/1520-0493(2002)130<1692:DSTOWT>2.0.CO;2

Markowski, P., & Richardson, Y. (2010). Hazards associated with deep moist convection. In *Mesoscale Meteorology in Midlatitudes* (pp. 273–313). Chichester, West Sussex, UK: John Wiley & Sons, Ltd.

Meng, Z., Bai, L., Zhang M., Wu, Z., Li, Z. Pu, M., et al., (2018). The deadliest tornado (EF4) in the past 40 years in China. *Weather and Forecasting*, **33**(3), 693–713. https://doi.org/10.1175/WAF-D-17-0085.1

Molina, M., & Allen, J. T. (2019). On the moisture origins of tornadic thunderstorms. *Journal of Climate*, *32*(14), 4321–4346. https://doi.org/10.1175/JCLI-D-18-0784.1

Molina, M., Allen, J., & Prein, A. (2020). Moisture attribution and sensitivity analysis of a winter tornado outbreak. *Weather and Forecasting*, **35**(4), 1263–1288. https://doi.org/10.1175/WAF-D-19-0240.1

Nie, Y., & Sun, J. (2022). Moisture sources and transport for extreme precipitation over Henan in July 2021. *Geophysical Research Letters*, *49*(4). https://doi.org/10.1029/2021GL097446

Rote, G. (1991). Computing the minimum Hausdorff distance between two point sets on a line under translation. *Information Processing Letters*, **38**(3), 123–127. https://doi.org/10.1016/0020-0190(91)90233-8

Seidel, D. J., Zhang, Y., Beljaars, A., Golaz, J., Jacobson, A. R., & Medeiros, B. (2012). Climatology of the planetary boundary layer over the continental Unitied States and Europe. *Journal of Geophysical Research: Atmospheres*, **117**(D17), D17106. https://doi.org/10.1029/2012JD018143

Sodemann, H., Schwierz, C., & Wernli, H. (2008). Interannual variability of Greenland winter precipitation sources: Lagrangian moisture diagnostic and North Atlantic Oscillation influence. *Journal of Geophysical Research: Atmospheres*, **113**(D3), D03107. https://doi.org/10.1029/2007JD008503

Sprenger, M., & Wernli, H. (2015). The LAGRANTO Lagrangian analysis tool – version 2.0. *Geoscientific Model Development*, **8**(8), 2569–2586. https://doi.org/10.5194/gmd-8-2569-2015

Stein, A., Draxler, R. R., Rolph, G. D., Stunder, B. J., Cohen, M., & Ngan, F. (2015). NOAA's HYSPLIT atmospheric transport and dispersion modeling system. *Bulletin of the American Meteorological Society*, **96**(12), 2059–2077. https://doi.org/10.1175/BAMS-D-14-00110.1

Stohl, A., Forster, C., Frank, A., Seibert, P., & Wotawa, G. (2005), Technical note: The Lagrangian particle dispersion model FLEXPART version 6.2, *Atmospheric Chemistry and Physics*, **5**(9), 4739–4754. https://doi.org/10.5194/acpd-5-4739-2005

Thompson, R. L., Edwards, R., Hart, J. A., Elmore, K. L., & Markowski, P. (2003). Close Proximity Soundings within Supercell Environments Obtained from the Rapid Update Cycle. *Weather and Forecasting*, **18**(6), 1243–1261. https://doi.org/10.1175/1520-0434(2003)018<1243:CPSWSE>2.0.CO;2

Trenberth, K., & Guillemot, C. (1995). Evaluation of the global atmospheric moisture budget as seen from analyses. *Journal of Climate,* **8**(9), 2255–2280. https://doi.org/10.1175/1520-0442(1995)008<2255:EOTGAM>2.0.CO;2

Wang, Y., Liu, X., Zhang, D., & Peng, B. (2023). Tracking moisture sources of precipitation over China. *Journal of Geophysical Research: Atmospheres,* **128**(15), e2023JD039106. https://doi.org/10.1029/2023JD039106

Warner, M. (2018). Introduction to PySPLIT: A python toolkit for NOAA ARL's HYSPLIT model. *Computing in Science & Engineering,* **20**(5), 47–62. https://doi.org/10.1109/MCSE.2017.3301549

Wilks, D. S. (2011). Statistical methods in the atmospheric sciences. In R. Dmowska, D. Hartmann, & H. T. Rossby (Eds.), Statistical methods in the atmospheric sciences (pp. 614). Academic Press. https://doi.org/10.1016/B978-0-12-385022-5.00015-4

Yang, Z., Huang, W., He, X., Wang, Y., Qiu, T., Wright, J., & Wang, B. (2019). Synoptic conditions and moisture sources for extreme snowfall events over East China. *Journal of Geophysical Research: Atmospheres,* **124**(2), 601–623. https://doi.org/10.1029/2018JD029280

Yao, S., & Jiang, D. (2023). Lagrangian simulations of moisture sources for Northeast China precipitation during 1979–2018. *Journal of Hydrometeorology*, **24**(12), 2225–2238. https://doi.org/10.1175/JHM-D-22-0201.1

Yu, X., Zhao, J., & Fan, W. (2021). Tornadoes in China: Spatiotemporal distribution and environmental characteristics. *Journal of Tropical Meteorology*, **37**(5/6), 681–692. https://doi.org/10.16032/j.issn.1004-4965.2021.064

Yuan, C., Yang, W., Li, D., Yang, L., & Wang, S. (2023). Climatology and environmental features of tornadoes in Liaoning Province during 1971–2020. Meteorological Monthly, **49**(11), 1285–1298. https://doi.org/10.7519/j.issn.1000-0526.2023.032601

Zhang, C., Xue, M., Zhu, K., & Yu, X. (2023). Climatology of significant tornadoes within China and comparison of tornado environments between the United States and China. *Monthly Weather Review*, **151**(2), 465–484. https://doi.org/10.1175/MWR-D-22-0070.1

Zhang, R., Xue, M. & Yu, X. (2025) Environments of tornadic and non-tornadic supercells in China and optimized significant tornado parameter for China region. *Quarterly Journal of the Royal Meteorological Society*, e5027. https://doi.org/10 .1002/qj.5027

Zheng, Y. (2020). Review of Climatology and Favorable Environmental Conditions of Tornado in China. *Advances in Meteorological Science and Technology*, **10**(6), 69–75. https://doi.org/10.3969/j.issn.2095-1973.2020.06.012

Zheng, Y., Zhu, W., Yao, D., Meng, Z., Xue, M., Zhao K., et al. (2016). Wind speed scales and rating of the intensity of the 23 June 2016 tornado in Funing County, Jiangsu province. *Meteorological Monthly*, **42**(11), 1289–1303. http://doi.org/10.7519/j.issn.1000-0526.2016.11.001

Zhi, J., Huang, X., Bai, L., Cai, K., Li, C., Li, Z., et al. (2022). Characteristics of Tornado Activity and Disaster Events in China in 2021. *Advances in Meteorological Science and Technology*, **12**(1), 26–36. https://doi.org/10.3969/j.issn.2095-1973.2022.01.004